LAWRENCE
LIVERMORE
NATIONAL
LABORATORY

LLNL-JRNL-418061

Laser Created Relativistic Positron Jets

H. Chen, S. C. Wilks, D. D. Meyerhofer, J. Bonlie, C. D. Chen, S. N. Chen, C. Courtois, L. Elberson, G. Gregori, W. Kruer, O. Landoas, J. Mithen, C. Murphy, P. Nilson, D. Price, M. Scheider, R. Shepherd, C. Stoeckl, M. Tabak, R. Tommasini, P. Beiersdorder

October 14, 2009

Physical Review Letters

Disclaimer

Laser Created Relativistic Positron Jets

Hui Chen[1], S. C. Wilks[1], D. D. Meyerhofer[2,3], J. Bonlie[1], C. D. Chen[1], S. N. Chen[1], C. Courtois[4], L. Elberson[1], G. Gregori[5], W. Kruer[1], O. Landoas[4], J. Mithen[5], C. Murphy[5], P. Nilson[2], D. Price[1], M. Schneider[1], R. Shepherd[1], C. Stoeckl[2], M. Tabak[1], R. Tommasini[1] and P. Beiersdorfer[1]

1. Lawrence Livermore National Laboratory, Livermore, CA 94551, USA

2. Laser Laboratory for Energetics, also at Department of Mechanical Engineering and Physics, University of Rochester, Rochester, NY 14623, USA

3. Department of Mechanical Engineering and Physics, University of Rochester, Rochester, NY 14623, USA

4. CEA, DAM, DIF, F-91297 Arpajon, France

5. Clarendon Laboratory, University of Oxford, OX1 3PU, UK

(10/13/09 11:38:24 AM)

Electron-positron jets with MeV temperature are thought to be present in a wide variety of astrophysical phenomena such as active galaxies, quasars, gamma ray bursts and black holes [1-4]. They have now been created in the laboratory in a controlled fashion by irradiating a gold target with an intense picosecond duration laser pulse. About 10^{11} MeV positrons are emitted from the rear surface of the target in a 15 to 22-degree cone for a duration comparable to the laser pulse. These positron jets are quasi-monoenergetic ($E/\delta E \sim 5$) with peak energies controllable from 3 – 19 MeV. They have temperatures from 1 – 4 MeV in the beam frame in both the longitudinal and transverse directions. Positron production has been studied extensively in recent decades at low energies (sub-MeV) in areas related to surface

science [5-8], positron emission tomography [9], basic antimatter science such as antihydrogen experiments [10, 11], Bose-Einstein condensed positronium [12], and basic plasma physics [13]. However, the experimental tools to produce very high temperature positrons and high-flux positron jets needed [14] to simulate astrophysical positron conditions have so far been absent. The MeV temperature jets of positrons and electrons produced in our experiments offer a first step to evaluate the physics models used to explain some of the most energetic phenomena in the universe.

Our electron-positron pair creation experiments were performed using 1-10 picosecond laser pulses of 1.054 μm wavelength from the Titan laser at the Lawrence Livermore National Laboratory and the OMEGA EP laser at University of Rochester's Laboratory for Laser Energetics. Laser energies from 100 J to 850 J was focused into 8 to 50 micrometer diameter spots producing peak laser intensities from 1×10^{19} to 5×10^{20} W/cm^2. All targets were 1 mm thick solid gold with diameters between 1 – 20 mm. The experimental configuration is shown in Fig. 1. The positrons, electrons and protons produced during the laser-target interaction were measured simultaneously using three absolutely calibrated electron-positron-proton spectrometers (EPPS) [15]. These EPPS's were placed ~ 20 cm from the target at various angles to measure the distribution of the electrons and positrons as a function of energy. The pair producing process in these experiments is the same as previous experiments [16-18]. When intense lasers interact with solid targets a large number of fast electrons (> MeV) are created. These electrons crate MeV Bremsstrahlung photons in the target that in turn produce electron-positron pairs

through the Bethe-Heitler process [19-21], unlike the direct laser pair production in vacuum through multiphoton absorption [22].

In the experiments described here, quasi-monoenergetic, beam-like positron jets were observed. The positron energy spectra are shown in Fig. 2 for six shots with different laser and target conditions that controlled the positron peak energy. The energy (E_{peak}) of the peak of the positron distribution varied from 3 to 19 MeV, with an energy spread from 57% to 15%, equivalent to E_{peak}/E_{FWHM}=1.8 to 6.9.

The positron beam energies were controlled by manipulating the sheath electric field at the back of the target. The sheath field is believed to be established by the escaping electrons and the fast electron cloud around the target, although the detailed physics of how and when the energetic electrons set up the sheath field is not known. At a strength of $\varepsilon \sim 1$ MeV/μm [23, 24], the sheath can easily accelerate positrons to MeV energies in similar fashion as the laser proton acceleration mechanism [25]. The sheath field relates to the electron temperature (T_e) and plasma scale length (L) of the target rear surface as $\varepsilon \propto T_e/eL$ [23]. T_e can be varied by selecting the pulse length and energy of the laser beam irradiating the front side of the target due to the dependence of the T_e on the laser intensity [26], while L is controlled by the injection of a second, long (ns) laser pulse, which irradiates the back side of the target [27]. The combination of short- and long-pulse lasers is key to manipulating the positron beam energy.

An additional handle to vary the positron acceleration field is the target size. By enlarging the size of the target we reduce the sheath acceleration field so that the positron

distribution approaches the low-energy limit determined by the Bethe-Heitler process [17], as shown in Fig. 3. The positron "birth" distribution given by the Bethe-Heitler process was simulated using the Monte-Carlo code EGSnrc [28], which calculates the Bethe-Heitler pair production and self-consistently treats the attenuation of electrons, photons, and positrons as they propagate through a cold solid target. It does not include the laser plasma effects that cause the additional acceleration of positrons at the rear target surface. The experimental data using a 20 mm diameter target has the lowest peak energy (~ 4 MeV) and is the closest to the simulated positron distribution peaked at about 2.5 MeV. Furthermore, the positron beam energy is approximately inversely proportional to the surface area of the target, as shown in the inset of Fig. 3. As the target diameter increases from 1 mm to 20 mm, the peak positron energy decreases from 18 MeV to 4 MeV. (For these shots, all laser parameters and the target thickness were kept constant.) Similarly, the measured maximum proton energy decreases from greater than 15 MeV to less than 0.5 MeV as the target diameter increases from 1 to 20 mm, consistent with the positron data. Since the electron source is the same for each target, the charge density is reduced as the target area increases, reducing the acceleration field as shown by the shift in the peak of positron energy to lower energies and the decrease in the maximum observed proton energy.

The jet nature of these quasi-monoenergetic positrons is established by measuring the beam angular divergence of electrons and positrons emitted from the rear surface of the target. Divergence angles were determined to range from 17º to 25º, with the smaller angles corresponding to the higher beam energies. Figure 4 shows measurements (for Shot B in Fig. 2) of the normalized total positron number as a function of angle with the laser

propagation direction at 0º and the target normal direction being –18º. A Gaussian function fit to the data indicating a width of ~20±5º centred at –10±5º. Fast electrons measured with the EPPS and radiochromic film show (in the inset of Fig. 3) a jet-like distribution similar to the positrons, with width of ~25±5º centered at –12±5º.

The physics that determines the electron directionality is different from that of the positrons. Fast electrons accelerated in front of the target are directed primarily along the laser axis, although a smaller fraction of fast electrons are driven by the $\mathbf{J}\times\mathbf{B}$ forces in the target-normal direction. Positrons are born deep inside the target and are predominantly from the most energetic electrons. At birth, these positrons carry some of the forward momentum of the "parent" fast electrons, and form a jet-like cone shape, as shown in the EGS simulation in Fig. 4. Once outside the target, these positrons are accelerated by the sheath electric field reshaping the positron distribution. This is verified by experiments with 18º and 55º laser incidence relative to target normal direction. It was found that the shots with nearer (18º) to laser normal incidence produced less divergent positron beams than those with 55º laser incidence, consistent with this argument.

The total number (N) of positrons in the jet is estimated to be on the order of 10^{10} to 10^{11} by integration over the angular spread of the jet. N scales approximately linearly with laser energy as $N \sim (1.5\times10^{11})\times E_{laser}(\text{kJ})$. The total energy conversion efficiency from laser energy to positrons in the jet is $\sim 2\times10^{-4}$. The positron jet current (~ 100 A) is far below the beam limit (~10,000 A) estimated by the Alfvén current [29]. Partial charge-neutrality was achieved in the jet of positrons with the co-propagating electrons. The electrons and positrons travel at nearly the velocity of light in the direction of the jet, ahead of the protons

and ions that are accelerated by the sheath electric field, forming a non-neutral electron-positron plasma due to the much higher electron number. For the duration of 10 picoseconds (laser duration), these relativistic electrons and positrons occupy a volume of $\sim 3\times10^{-3}$ cm^3, from which a positron density of $\sim 10^{13}$/cm^3 and electron density of $\sim 10^{15}$/cm^3 are inferred. EGS simulations show a positron density of $\sim 10^{16}$ cm^{-3} inside of the target.

The positron temperature is determined from the width of the energy spectrum in the jet, or longitudinal, direction and from the angular divergence of the jets in the transverse direction. In the longitudinal direction, the temperatures ($T_{//}$) are between 2 – 6 MeV. In the transverse direction, the temperatures ($T_{\perp}$) are between 0.4 – 2 MeV. The temperatures obtained in the EGS simulations (for Shot B) are 3.4 MeV and 1.4 MeV in the longitudinal and transverse directions, respectively. This agrees well with the experimental data. The co-propagating hot electron temperatures are about 3 to 9 MeV with a quasi Maxwellian distribution [18].

Presently these laboratory produced positron jets and plasmas cannot be directly compared to their astrophysical counterpart. Although the energy flux of these electron-positron jets is in the order of 10^{21} erg/s/cm^2, its power is only about 10^{19} erg/s that is far less than that of astrophysical sources [1-4]. The potential of this laboratory source may be realized in scaled experiments [30]. The quasi-monoenergetic feature of these positron jets may enable the creation of MeV temperature electron-positron plasmas if they can be trapped, for example in a “mirror-type” magnetic field [21]. With the beam intensity about

10^{12} W/cm^2, these positrons may also find new applications such as diagnosing high energy density plasmas as well as providing a source of pulsed, monoenergetic gamma rays for radiography of dynamic processes in materials.

1. J. Wardle, et al., Nature **395**, 457 (1998)
2. I. F. Mirabel and L. F. Rodriguez, Review of Astronomy and Astrophysics **37**, 409-43 (1999).
3. G. Weidenspointner et al, Nature **451**, 159, 2008
4. P. Meszaros, Annal Review of Astronomy and Astrophysics **40**, 137 (2002).
5. A. P. Mills, Science **218**, 335 (1982)
6. P. J. Schultz and K. G. Lynn, Rev. Mod. Phys. **60**, 701 (1988)
7. A.W. Hunt, et al, Nature **402**, 157, 1999
8. D. W. Gidley, H-G Peng and R. S. Vallery, Annal Review of Mater. Res. **36**, 49-79 (2006).
9. M. E. Raichle, Nature **317**, 574 (1985)
10. M. Amoretti, et al, Nature **419**, 456-459 (2002)
11. G. Gabrielse et al., Phys. Rev. Lett, **89**, 213401 (2002)
12. P. M. Platzman and A. P. Mills, Phys. Rev. B **49**, 454 (1994)
13. C. M. Surko and R. G. Greaves, Physics of Plasmas **11**, 2333 (2004)
14. M. H. Thoma, Rev. Mod. Phys. **81**, 959 (2009) and references cited within.
15. H. Chen, et al., Rev. Sci. Instrum. **79**, 10E533 (2008).
16. T. Cowan, et al., Laser Particle Beams **17**, 773 (1999)
17. C. Gahn, et al., Appl. Phys. Lett. **77**, 2662 (2000)
18. Hui Chen et al., Phys. Rev. Lett. **102**, 105001 (2009)
19. W. Heitler, The Quantum Theory of Radiation (Clarendon Press, Oxford, 1954)
20. K. Nakashima and H. Takabe, Phys. Plasmas 9, 1505 (2002).
21. J. Myatt, et al., Phys. Rev. E 79, 066409 (2009).
22. D. L. Burke, et al., Phys. Rev. Lett. **79**, 1626 (1997)

23. S. P. Hatchett et al., Phys. Plasmas **7**, 2076 (2000)

24. S. C. Wilks, et~al., Phys. Plasmas **8**, 542 (2001)

25. R. A. Snavely, et al. Phys. Rev. Lett. **44**, 229 (1999)

26. S. C. Wilks et al. Phys. Rev. Lett. **69**, 1383 (1992)

27. A. J. Mackinnon, et al. Phys. Rev. Lett. **86**, 1769 (2001)

28. I. Kawrakow and D. W. O. Rogers, National Research Council of Canada Report PIRS-701 (2006).

29. H. Alfvén, Phys. Rev. **55** 425 (1939)

30. B. A Remington, D. Arnett, R. P. Drake, and H. Takabe, Science **284**, 1488 (1999)

Acknowledgements This work was performed under the auspices of the U.S. DOE by LLNL under Contract DE-AC52-07NA27344 and DE-FC52-08NA28302, and was funded with LLNL LDRD-08-LW-058 and ILSA. We thank the LLNL Jupiter Laser Facility and the LLE OMEGA EP laser. We acknowledge support from Roger Van Maren, Don Correll and Bill Goldstein, and discussions with Peter Norreys and Robert Heeter.

Author Contributions H.C. led the experiments and performed the main analysis. S.W. helped with the shot planning and performed the EGS simulations. D.M. and P.B critically discussed the analysis and paper layout. J.B., C.C., S.C., L.E., G.G., J.M., C.M., D.P., M.S., R.S. and R.T. contributed to the Titan experiments. C.C., O.L., P.N., and C.S. contributed in the OMEGA EP experiments. S.W., W.K. and M.T contributed to the theoretical interpretation of the results.

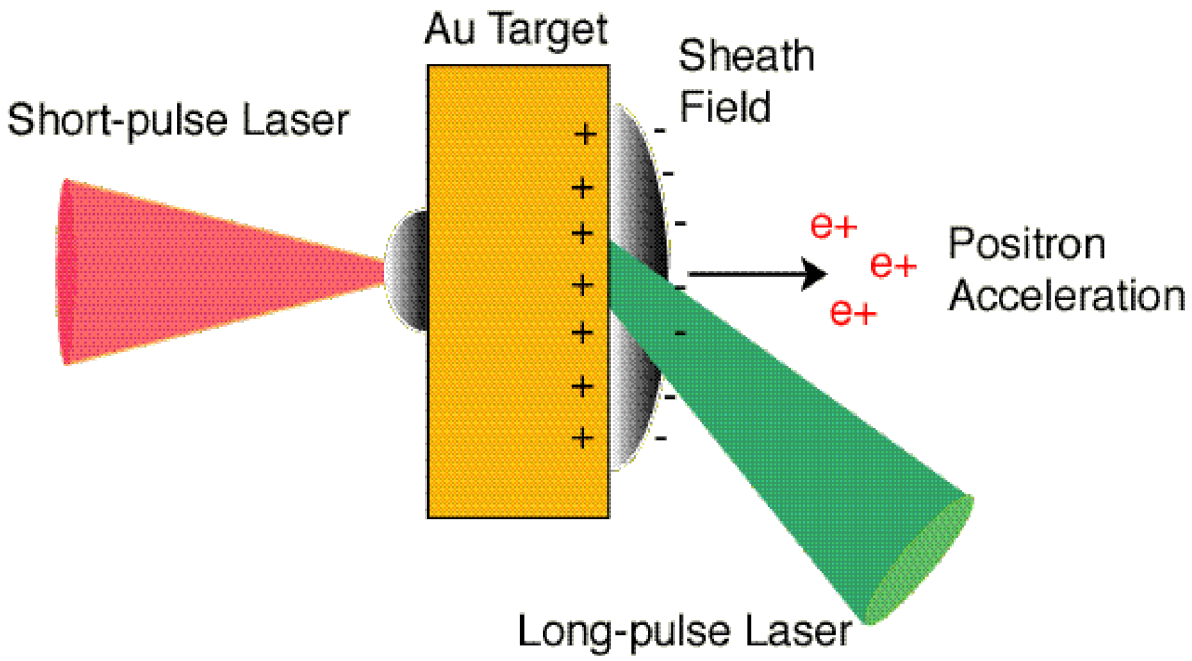

Fig. 1. Illustration of the experimental setup. The short pulse irradiates the target at 18^{o} relative to target normal. The long pulse (LP) (3 ns square pulse) laser irradiates the rear of the target at 45^{o}. The LP was shot 2 ns before the short pulse laser. The LP focal spot was about 600 mm diameter centered on the short pulse focal spot. The laser produced electrons establish a sheath field at the rear of the target that can accelerate positrons. This field can be controlled by the long-pulse laser injection as well as the target surface area variation.

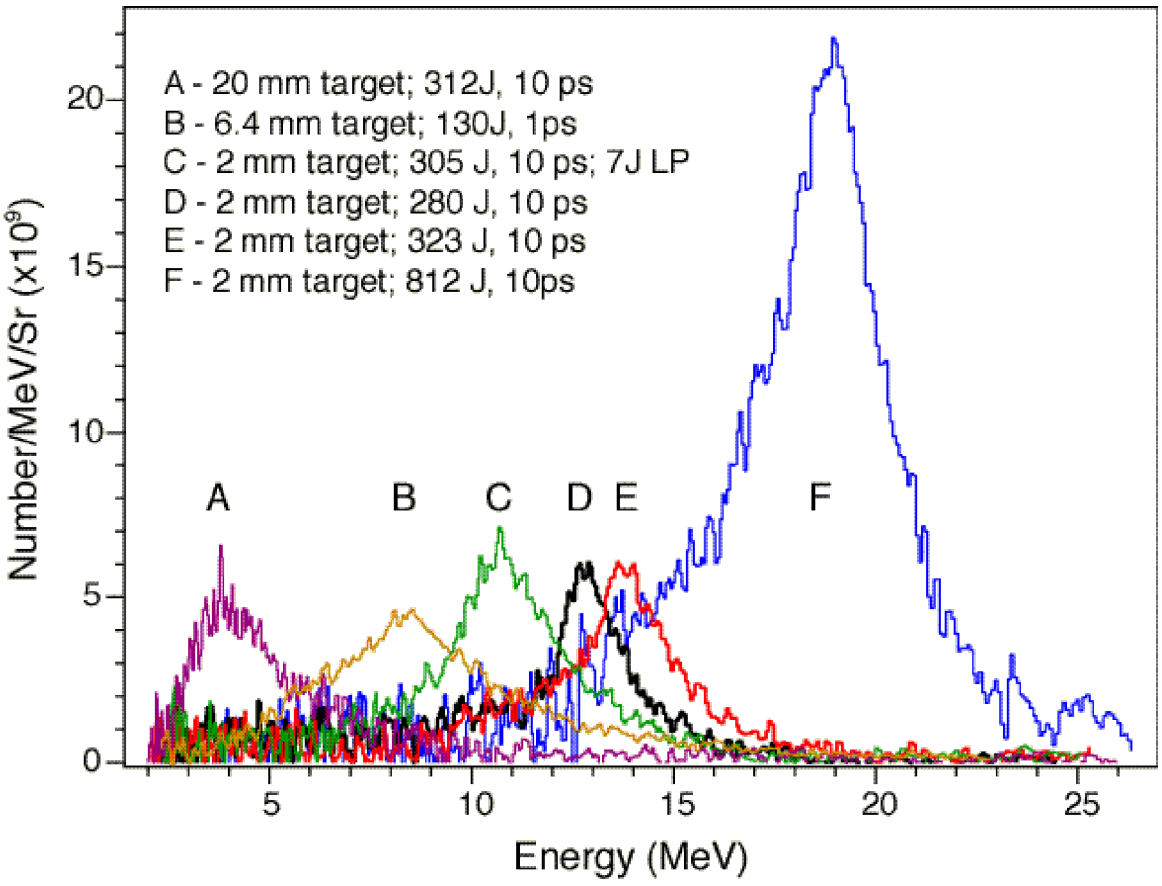

Fig. 2 Positron energy distributions for six laser shots labelled from A to F. The target and laser conditions are listed. Shots A-E were from Titan laser and Shot E from OMEGA EP laser. All spectra were obtained with the EPPS observing normal to the back of target.

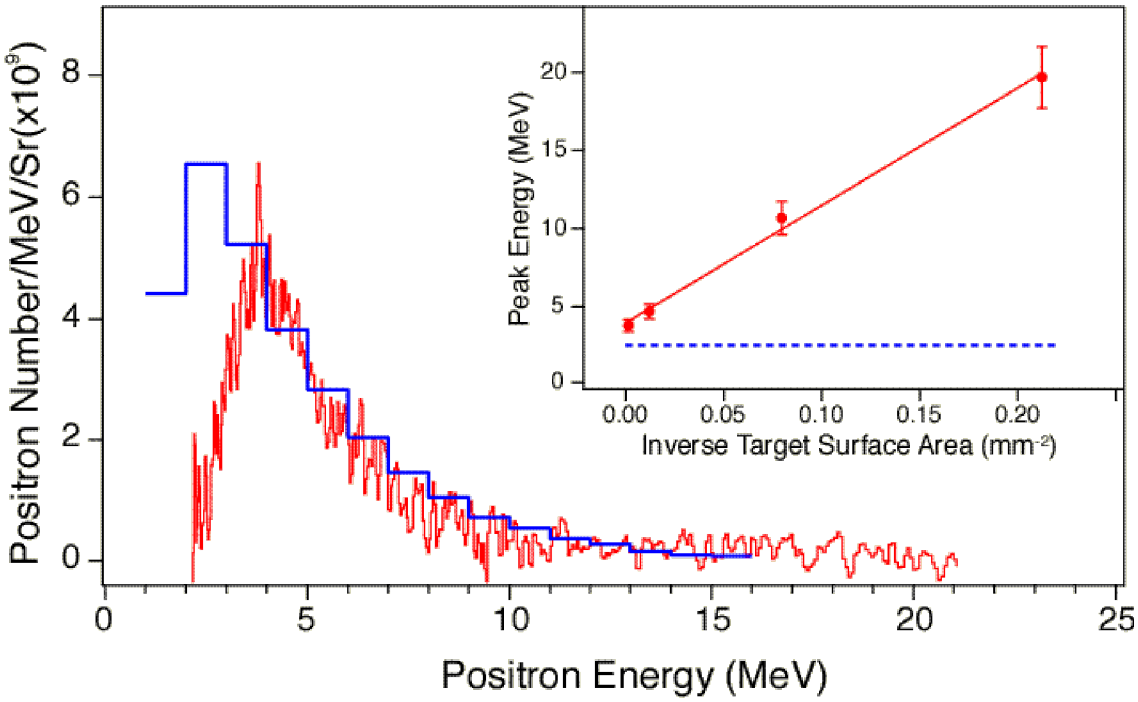

Fig. 3 Positron spectra from 1 mm thick Au targets with diameters of 20 mm (red) and from EGS code (blue). The simulation is linearly scaled with an arbitrarily factor in the y-axis to show its peak energy. Shown in the inset is the peak energy of positrons as a function of the inverse of target surface areas. The relation is fitted with a linear function $E \propto 1/S$. The dashed line (blue) represents the peak energy without the acceleration field, calculated from the EGS simulation.

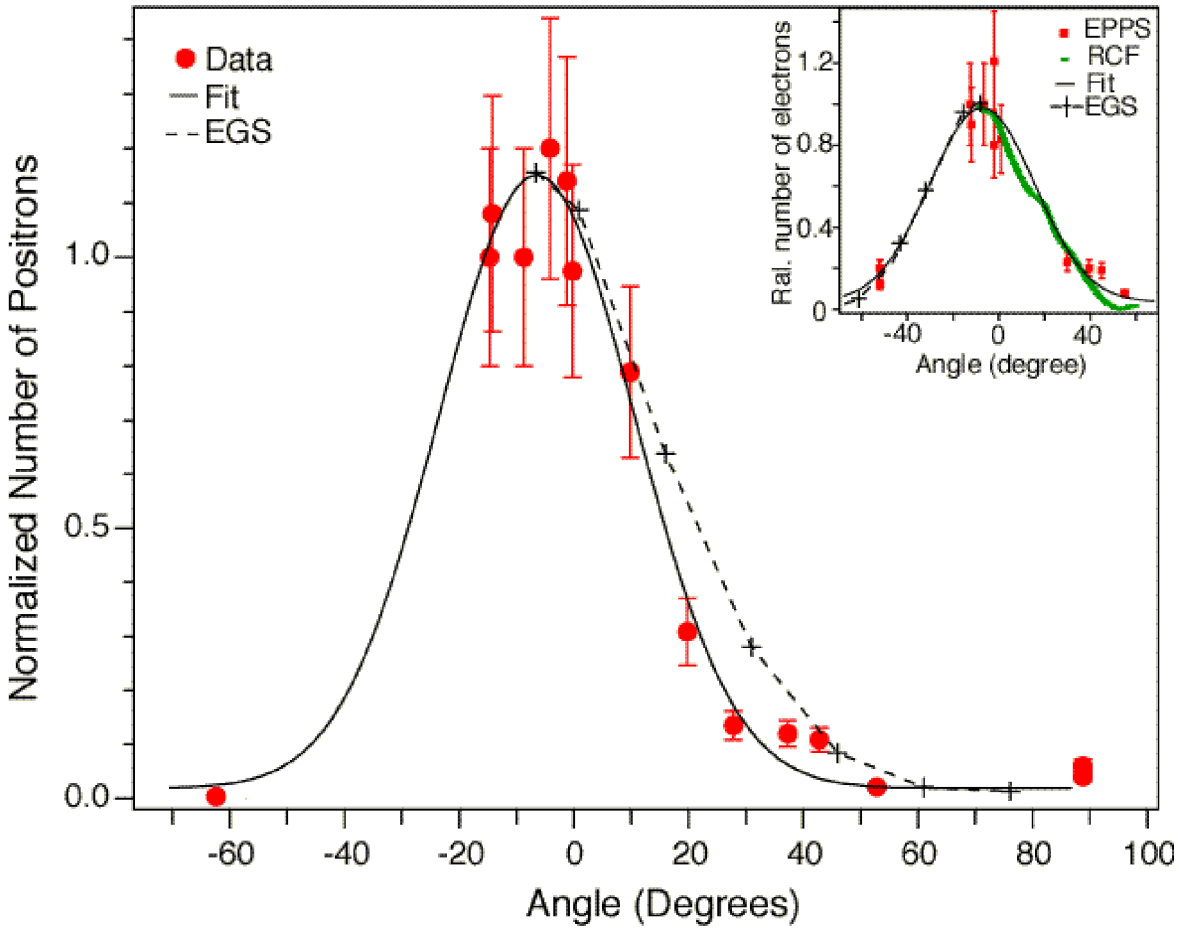

Fig. 4 Normalized total positron number ejected from the back of targets at various angles for 1 mm thick, 6.4 mm diameter targets shot by 1 ps, 130 J laser (Shot B in Fig. 2). The data (red dots with error bars) is fit (black) with a Gaussian function. The result for the electrons is shown inset including both EPPS data (red squares) and data from radiochromic film (green dots). The angular distribution calculated using the EGS simulations is shown as the dashed curve with crosses for both positrons and electrons. It was not possible to measure positrons for angles between –60º and –20º due to the laser beam layout.